Isothermal evolution of phase composition, structural parameters, and ionic conductivity in $Na_{1+x}Al_xGe_{2-x}(PO_4)_3$ Glass-Ceramics

Jairo F. Ortiz-Mosquera [1], Adriana M. Nieto-Muñoz [1], Henrik Bradtmüller [2], Hellmut Eckert[2,3], and Ana C. M. Rodrigues[4]

1. Programa de Pós-Graduação em Ciência e Engenharia de Materiais, Universidade Federal de São Carlos, CP 676, 13565-905, São Carlos, SP, Brazil

2. Institut für Physikalische Chemie, WWU Münster, Corrensstraße 30, D48149 Münster, Germany

3. Instituto de Física de São Carlos, Universidade de São Paulo, CP 369, 13566-590, São Carlos, SP, Brazil

4. Departamento de Engenharia de Materiais, Universidade Federal de São Carlos, CP 676, 13565-905, São Carlos, SP, Brazil

ABSTRACT

Precursor glasses with composition $Na_{1+x}Al_xGe_{2-x}(PO_4)_3$ (NAGP) ($0.6 \leq x \leq 1.0$) are converted into Na-Super ion conductor (NASICON) glass-ceramics by thermal treatments with varied duration and annealing temperature. Detailed X-ray powder diffraction with Rietveld refinement and ^{31}P and ^{27}Al solid state nuclear magnetic resonance (NMR) spectroscopy show that extended annealing at the crystallization temperature leads to a progressive de-alumination, segregation of T-$AlPO_4$ and other crystalline phases, accompanied by the formation of amorphous material. These results suggest that an earlier formed aluminum super-saturated structure equilibrates by losing aluminum upon extended annealing. However, the glass-ceramics ionic conductivity is less affected than would be predicted by the Al loss encountered in the NASICON phase, suggesting that ionic conductivity in the glass-ceramics is not controlled by the composition of the NASICON phase alone but is further influenced by the other phases present, either by contributing directly to ion transport or by facilitating interparticle contacts.

Keywords: Glass-ceramics; NASICON structure; solid state NMR; ionic conductivity; Rietveld analysis; glass crystallization

Introduction

Meeting the growing demands of energy for mobile and stationary equipment is a key challenge to ensure the sustainability of our current society. While lithium ion batteries are well accepted in the market, the limited abundance of lithium and its rather restricted geographical distribution mandate the search for new and less expensive alternatives. Sodium represents a natural possible substitute to lithium in stationary power storage applications. It is the 4th most abundant element in the earth's crust, thus widely distributed all over the world and its oxidation potential is still quite attractive. In fact, sodium batteries for use at high and low temperatures have already been widely investigated [1,2]. All-solid-state batteries using solid instead of liquid electrolytes are of particular interest from the viewpoints of operating safety, and energy density optimization [3–5]. Among the large group of inorganic solid electrolytes, those featuring a crystal structure with 3-D interconnected open channels possess particularly high ionic conductivity [6]. Compounds with the NASICON (**Na**-**S**uper **I**onic **C**onductor) structure and general formula $A(I)_{1+2w+x-y+z}M(II)_wM(III)_xM(V)_yM(IV)_{2-w-x-y}(SiO_4)_z(PO_4)_{3-z}$ are particularly suitable in this regard and have been widely studied in this connection [7,8]. The NASICON structure is composed of PO_4 tetrahedra linked via corners to MO_6 octahedra giving rise to three-dimensional open channels [9,10]. The structure accepts a wide range of iso- and aliovalent substitutions [2] on the basis of which several promising systems using Na^+ ions as charge carriers have been identified: $Na_{1+x}T_xM_{2-x}P_3O_{12}$, (T = Al^{+3}, Cr^{+3}, M = Ge^{+4}, Ti^{+4}, Hf^{+4}, Sn^{+4} and Zr^{+4}) and prepared by powder ceramic routes [11–13]. However, the employed sintering method may result in great porosity. Alternatively, the glass-ceramics route, i.e., the controlled crystallization of a precursor glass has been proposed for the synthesis of NASICON compounds [14–16], with the main advantages of reducing porosity and the control of microstructure [17]. It has already been pointed out that different temperatures of heat-treatment of crystallization may induce changes in the microstructure [15] and composition [18] of the corresponding glass-ceramics. However, the evolution of annealing effects caused by isothermal heat-treatments for controlled crystallization has been scarcely investigated. Short annealing times carry the risk of having a low fraction of crystalline material, leaving a substantial amount of Na^+ ions in the poorly conducting glassy phase. On the other hand, long annealing times and/or higher annealing temperatures may lead to decomposition and formation of other, non-conducting, crystalline phases. For developing optimum crystallization conditions, we need to identify the compositional and structural factors controlling ionic conductivity in these glass-ceramics. In the present study we address this question on glass-ceramics close to the solubility limit in the system $Na_{1+x}Al_xGe_{2-x}(PO_4)_3$. For samples with x =

0.8 and 1.0 the structural evolution in two different temperatures has been studied by X-ray diffraction (XRD) followed by Rietveld refinement. Ionic conductivity was measured by impedance spectroscopy. The results are also discussed in the context of the microstructural characteristics probed via Scanning Electron Microscopy (SEM). Nuclear Magnetic Resonance (NMR) spectroscopy on samples with x = 0.6, 0.8 and 1.0, allowed us to propose a model for the observed de-alumination process occurring during isothermal annealing of investigated glass-ceramics.

Experimental Section

Synthesis procedures

The $Na_{1+x}Al_xGe_{2-x}(PO_4)_3$ (x = 0.6, 0.8 and 1.0) parent glasses were prepared using the conventional melt-quenching method. The raw materials Na_2CO_3 (Vetec, 99,5%) GeO_2 (Aldrich, 99.9%), Al_2O_3 (Aldrich, 99.9%), and $(NH_4)_2HPO_4$ (Aldrich, 98%) were weighed and ball-milled with Al_2O_3 balls during 12 hrs. The batches were placed into platinum crucibles and heated to 400 °C and 700 °C during 2 h and 4 h, respectively, to decompose the starting materials, leading to the release of NH_3, H_2O and CO_2. Subsequently, the batches were melted at 1200 to 1280 °C for 30 minutes and the liquids were splat-cooled between two steel plates. The resultant glasses were annealed at T_g – 40 K during 2h, (520 °C for $Na_{1.4}Al_{0.6}Ge_{1.2}(PO_4)_3$, 500 °C for $Na_{1.8}Al_{0.8}Ge_{1.2}(PO_4)_3$, and 481 °C for $Na_2AlGe(PO_4)_3$) to release thermal stresses and then cooled down to room temperature.

In order to obtain the glass-ceramics, the parent glasses were crystallized by heat treatment at their crystallization temperatures T_x (T_x = 644 °C for x = 0.6 and 646 °C for x = 0.8 and 1.0, [19]) for 0.5 h, 3 h, 6 h, 24 h and at 800 °C for 3 h.

Analysis techniques

X-Ray Powder Diffraction. The powder patterns were collected at room temperature in a Rigaku Ultima IV X-ray diffractometer operating with CuK_α radiation generated at 20 mA and 40 kV. Data were recorded between 10 and 80 ° with 0.02 ° step size and 0.6 s counting time to identify the crystalline phases present in glass-ceramics. To refine the crystal structures by the Rietveld method, data were collected with 0.02 ° step size and 0.1 s counting time. The powder patterns were indexed using the Crystallographica Search-Match software [20] and

were analyzed by Rietveld refinements using the version 6 of TOPAS-Academic [21] in combination with the Inorganic Crystal Structure Database (ICSD) [22]. Rietveld refinements allowed the determination of the lattice parameters and the quantification of the crystalline phases present in the glass-ceramics.

MAS NMR Characterization. Multinuclear NMR spectroscopy was performed on the glass-ceramics with a BRUKER DSX-500 spectrometer operating at 11.7 T, BRUKER DSX-400 at 9.4 T and AGILENT 240-MR DD2 equipment, operating at 5.7 T. Commercial 4 mm triple resonance magic angle spinning (MAS) probes were used, operated at spinning rates between 10.0 and 15.0 kHz. ^{31}P MAS-NMR spectra were obtained at 98.12 MHz with π/2-pulses of 4.0 µs length and recycle delays of 1200 to 1400 s. The spectra were deconvoluted into Gaussian components. Assignments were assisted by ^{31}P{^{27}Al} Rotational Echo Adiabatic Passage Double Resonance (REAPDOR) experiments, conducted at 9.4 T, on samples rotating at 11.5 kHz, using nutation frequencies of 70 and 60 kHz on ^{31}P and ^{27}Al, respectively, and a relaxation delay of 700 – 900 s. Dipolar recoupling was effected by ^{27}Al irradiation during 1/3 of the rotor cycle. A dipolar recoupling period of 2.96 ms was chosen. ^{27}Al MAS-NMR studies were conducted at 63.1 MHz at 15.0 kHz spinning frequency. Single-pulse spectra were acquired using short pulses of 1.0 µs length and relaxation delays of 1s or less. Data processing and spectral simulations were carried out using the DMFIT program [23]. ^{27}Al{^{31}P} rotational echo double resonance experiments were conducted at 9.4 T, on samples rotating at 11.5 kHz, using nutation frequencies of 70 and 60 kHz on ^{31}P and ^{27}Al, respectively, and a relaxation delay of 0.5 s. Dipolar recoupling was effected by ^{31}P π pulses of 7.4 µs length during the rotor cycle. A dipolar recoupling period of 2.61 ms was chosen.

Microstructural Analysis. The microstructure of $Na_{1.8}Al_{0.8}Ge_{1.2}(PO_4)_3$ and $Na_2AlGe(PO_4)_3$ glass-ceramics were observed on fracture surfaces using a Phillips XL30 FEG Scanning Electron microscope,

Conductivity measurements. Ionic conductivities of the $Na_{1+x}Al_xGe_{2-x}(PO_4)_3$ (x = 0.8 and x = 1.0) glass-ceramics were measured by impedance spectroscopy. Samples with thicknesses varying from 1 to 2 mm and surface area around 25 mm^2 were polished and gold blocking electrodes were sputtered on both parallel sides with a QUORUM Q150R ES equipment. AC-impedance measurements were performed in the frequency range of 1 MHz to 0.1 Hz with voltage amplitude of 300 mV using a NOVOCONTROL Alpha-A High-Performance Frequency Analyzer in the temperature range of 50 to 300 °C. Measurement temperatures were adjusted within a precision of ± 0.1 °C using a NOVOTHERM furnace.

Results and Discussion

X-ray and Rietveld Refinement. Figure 1 shows the XRD powder patterns of $Na_{1.8}Al_{0.8}Ge_{1.2}(PO_4)_3$ (x = 0.8), and $Na_2AlGe(PO_4)_3$ (x = 1.0) glass-ceramics obtained after heat treatments of the parent glasses at T_x (646 °C) for 0.5 h, 3 h, 6 h, 24 h and at 800 °C for 3 h. While the main phase formed is the NASICON-type structure (space group $R\bar{3}$ ICSD 164019), triclinic $AlPO_4$ (ICSD: 280307) is observed as a secondary phase in all of the samples with x = 0.8 except for that heated for 30 minutes. In addition, the $Na_{1.8}Al_{0.8}Ge_{1.2}(PO_4)_3$ sample heated at T_x for 6 h shows a small amount of $Na_7(AlP_2O_7)_4PO_4$ (ICSD: 261924), which is absent in the all of the other samples. It might be argued that $Na_7(AlP_2O_7)_4PO_4$ appears as a metastable phase in this system at this particular heat treatment condition. In the case of the $Na_2AlGe(PO_4)_3$ samples, $AlPO_4$ phases are detected in all the glass-ceramics, both in the triclinic (ICSD: 280307) and hexagonal (ICSD: 9641) crystal systems, and $Na_7(AlP_2O_7)_4PO_4$ is more prominently observed in the samples heated at T_x for 6h and 24h. For the latter sample, reflexes owing to crystalline GeO_2 (ICSD: 59624) are observed as well. All of these results are consistent with our previous conclusion that at a composition of x = 0.8 the solubility limit of Al in the nominal $Na_{1+x}Al_xGe_{2-x}(PO_4)_3$ ($0 \le x \le 1.0$) system is reached [19].

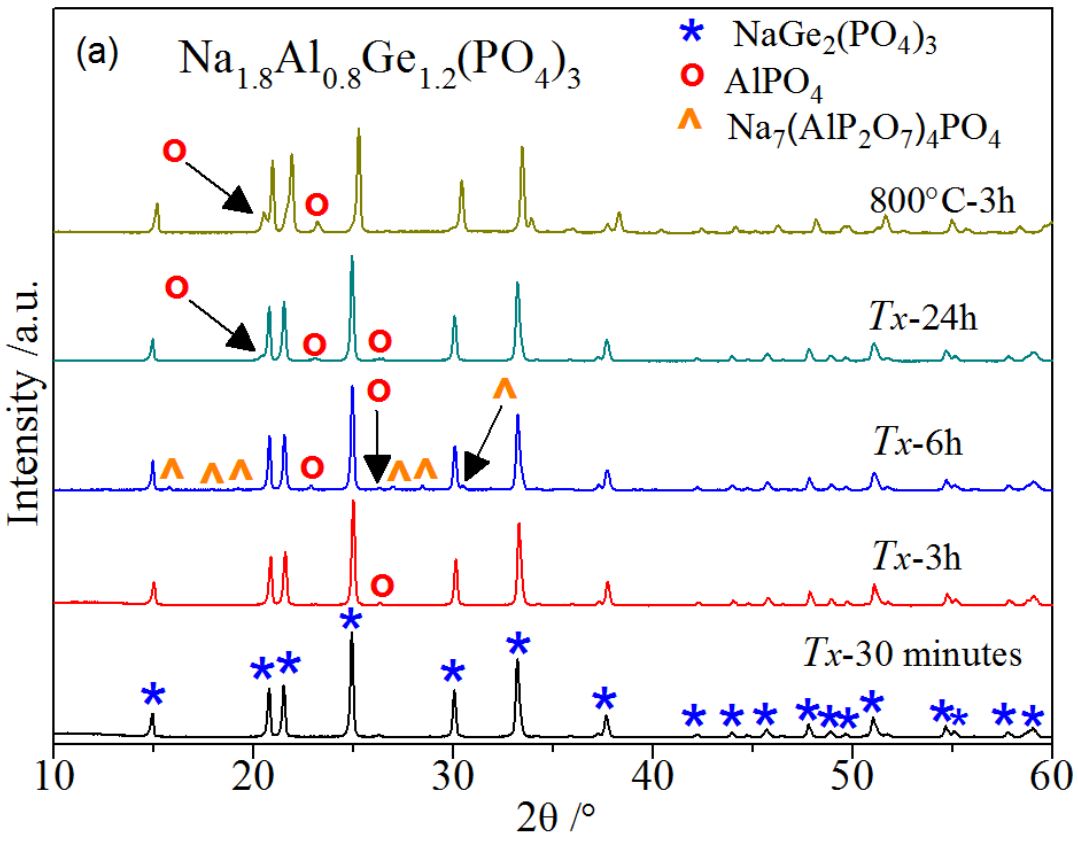

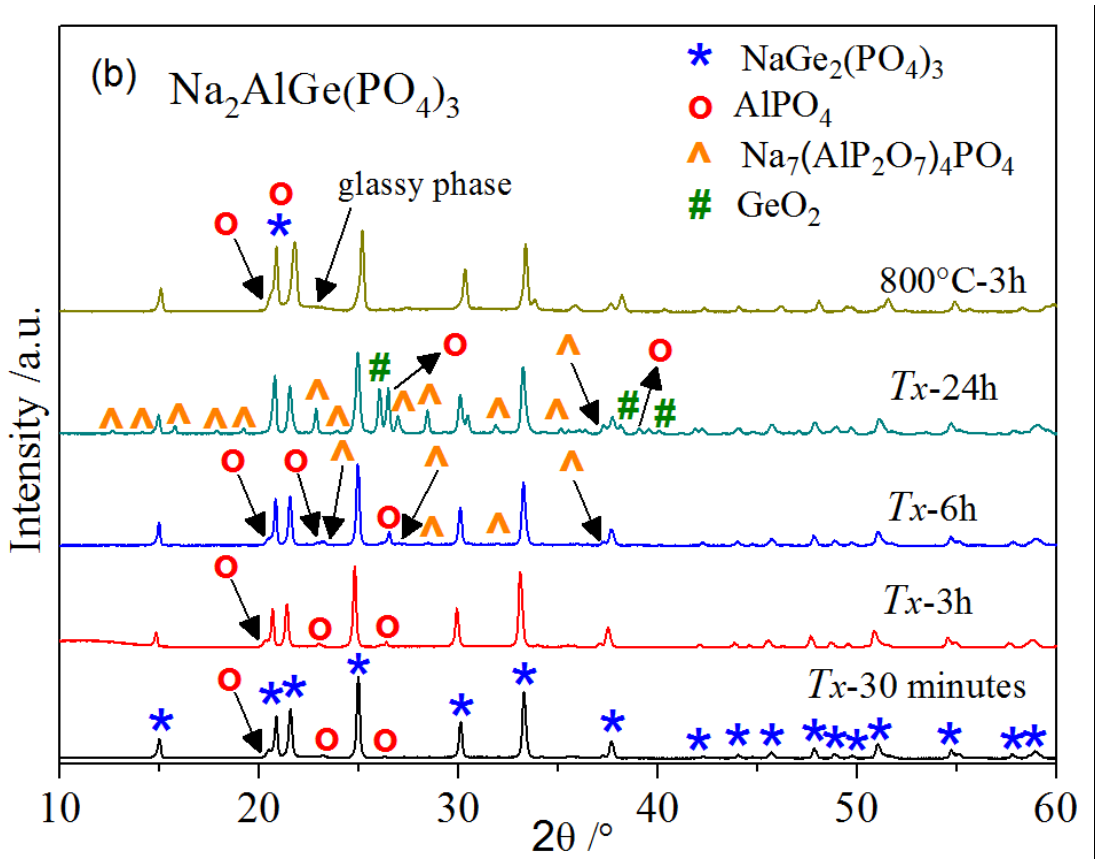

Figure 1. X-ray diffraction pattern of (a) $Na_{1.8}Al_{0.8}Ge_{1.2}(PO_4)_3$ and (b) $Na_2AlGe(PO_4)_3$ glass-ceramics, obtained after heat treatment of parent glasses at T_x (646°C) for 0.5 h, 3 h, 6 h, 24 h and at 800°C for 3 h.

Table 1. Lattice constants ($a = b$, c) and unit cell volumes of the NASICON structure, quantification of crystalline phases and agreement factor R_{wp} derived from Rietveld analysis. The numbers in parentheses indicate the mathematical errors given by Rietveld refinement.

T.T.	***a* (Å)**	***c* (Å)**	***V*(Å^3)**	**% $NaGe_2(PO_4)_3$**	**% $AlPO_4$-T**	**% $AlPO_4$-H**	**% $Na_7(AlP_2O_7)_4PO$**	**% GeO_2**	**% R_{wp}**
Glass-ceramics $Na_{1.8}Al_{0.8}Ge_{1.2}(PO_4)_3$									
T_x/30 min	8.2812(3)	21.3861(8)	1270.1(1)	100.0	0	0	0	0	15.9
T_x/3 h	8.2848(4)	21.3810(9)	1270.9(1)	98.0	2.0	0	0	0	14.2
T_x/6 h	8.2722(3)	21.3883(9)	1267.5(1)	86.9	2.0	0	11.1	0	15.2
T_x/24 h	8.2738(3)	21.3829(9)	1267.7(1)	92.9	7.1	0	0	0	15.3
800 °C/3 h	8.1677(2)	21.4365(7)	1238.5(1)	81.3	18.7	0	0	0	10.7
Glass-ceramics $Na_2AlGe(PO_4)_3$									
T_x/30 min	8.2955(4)	21.3703(9)	1273.6(1)	93.1	6.9	0	0	0	13.5
T_x/3 h	8.2978(4)	21.3796(9)	1274.8(1)	87.2	9.2	2.9	0	0	13.6
T_x/6 h	8.2842(4)	21.3699(9)	1270.1(1)	79.1	9.8	5.4	5.7	0	13.4

T_x/24 h	8.2590(4)	21.3695(9)	1262.4(1)	48.9	0	13.2	30.9	7.0	10.9
800 °C/3 h	8.1690(4)	21.4146(9)	1237.6(1)	82.8	17.2	0	0	0	11.50

* $R_{wp} = \Sigma [w(y_o - y_c)^2/\Sigma w y_o^2]^{1/2}$ y_o = Intensity of X-ray pattern observed, y_c = Intensity of X-ray pattern calculated, $w = 1/y_o$.

Table 1 and Figure 2 shows the percentages of the crystalline phases observed in $Na_{1.8}Al_{0.8}Ge_{1.2}(PO_4)_3$ (a) and $Na_2AlGe(PO_4)$ (b) glass-ceramics. The results illustrate the increasing extent of decomposition of the NASICON phase leading to the formation of secondary phases, with increasing annealing time at T_x. For the x = 1.0 sample treated for 24 h only about 50% of the material remains in the NASICON structure, whereas for x = 0.8 still 90% of NASICON phase is observed after 24 h at T_x. Figure 3 illustrates a successive decrease in the NASICON unit cell volume concomitant to the time of the thermal treatment. Again, this change is more pronounced in the x = 1.0 sample than in the x = 0.8 sample. Finally, in both the $Na_{1.8}Al_{0.8}Ge_{1.2}(PO_4)_3$ and $Na_2AlGe(PO_4)_3$ glass ceramics, heated at 800 °C for 3 h, the NASICON phase remains the major component (more than 80%), albeit with a drastically decreased cell volume.

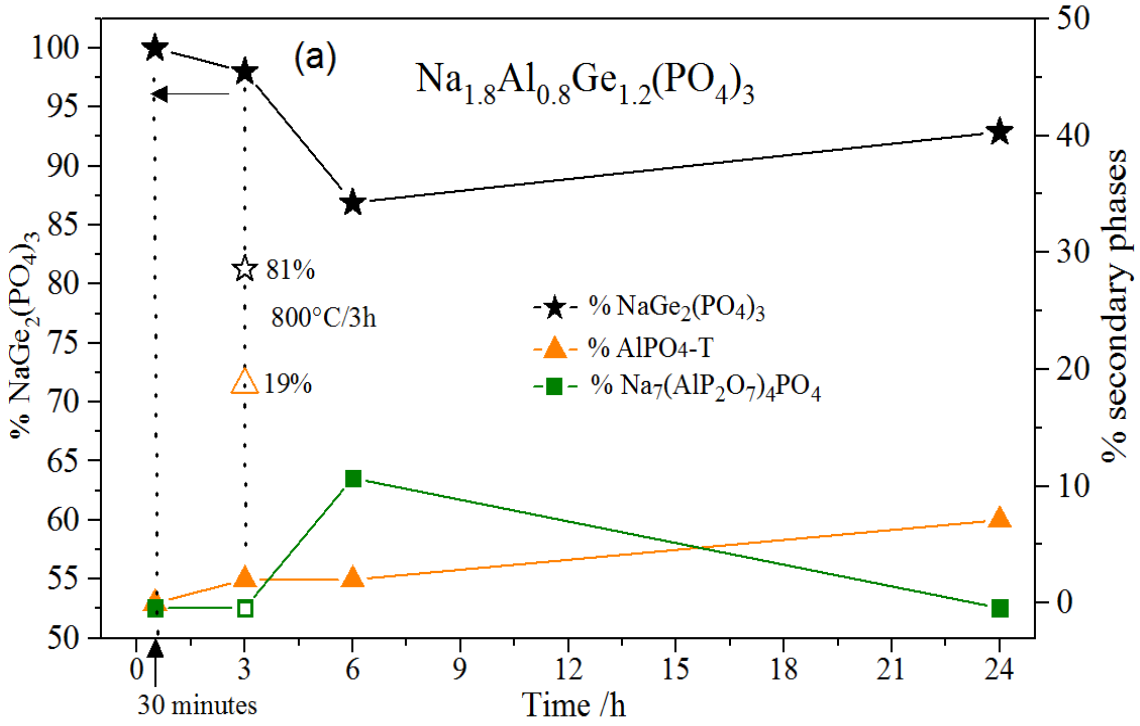

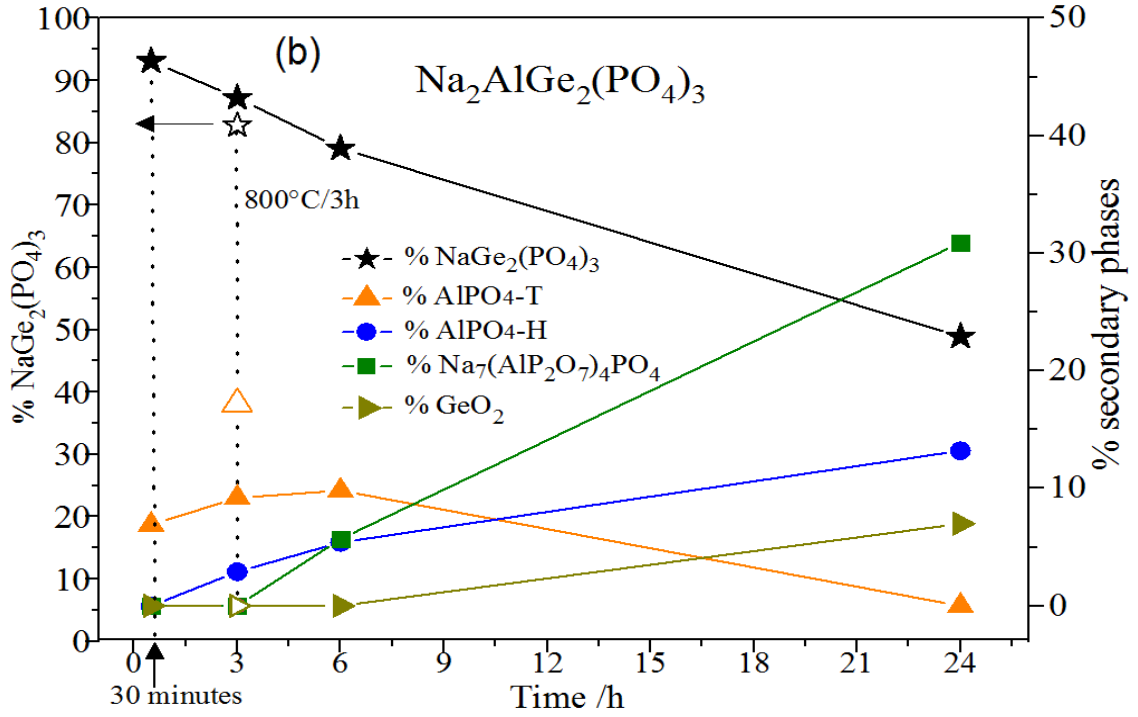

Figure 2. Percentages of crystalline phase quantified from Rietveld refinement, as a function of the time of heat treatment performed at T_x (646 °C) and 800 °C for (a) $Na_{1.8}Al_{0.8}Ge_{1.2}(PO_4)_3$ and (b) $Na_2AlGe(PO_4)_3$ glass-ceramics. The unfilled symbols correspond to the values found for sample crystallized at 800 °C for 3 h. Lines are guide to the eyes.

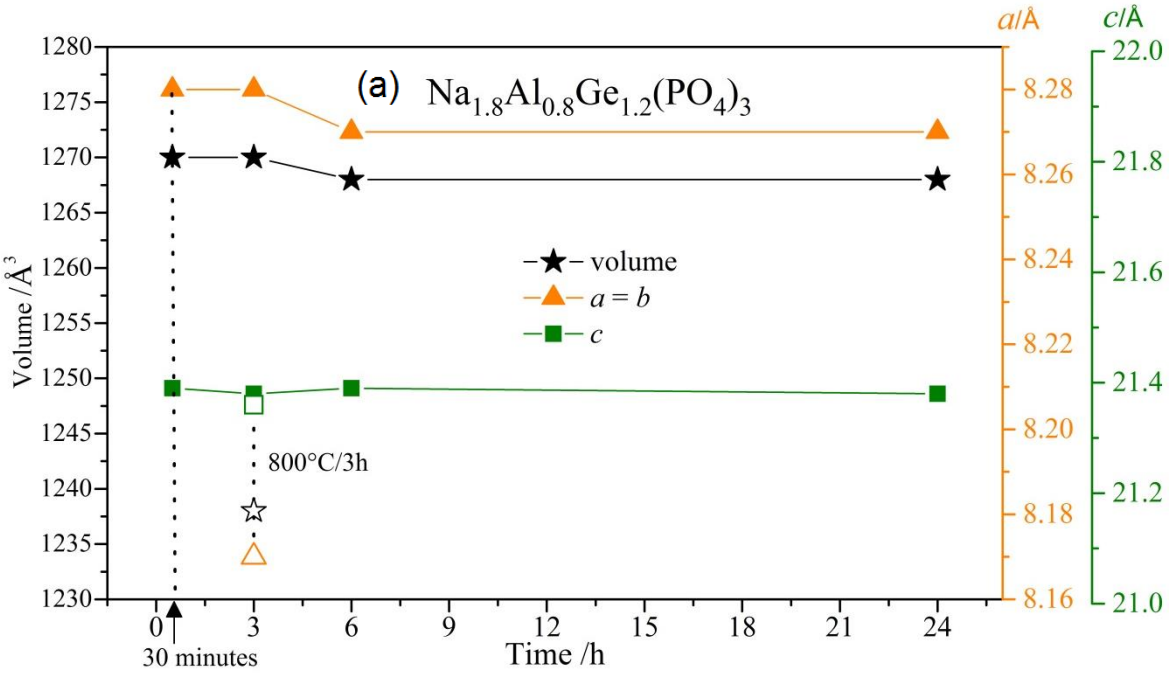

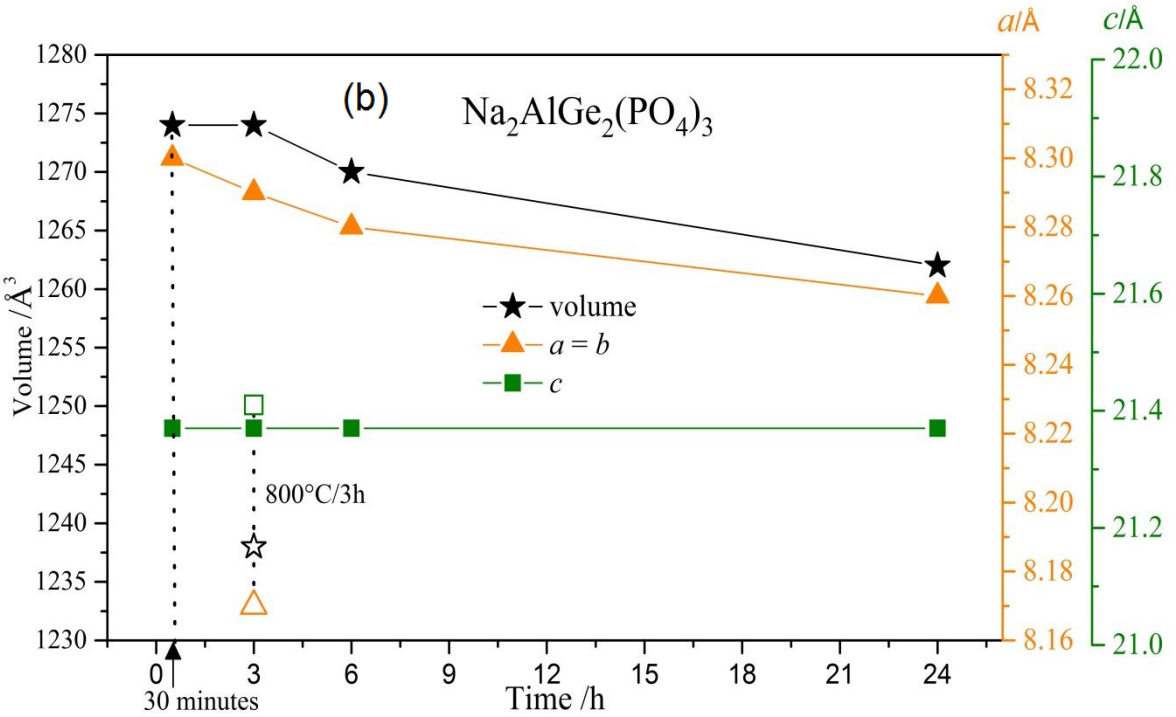

Figure 3. Variation of lattice constants and unit cell volumes of the NASICON structure, as a function of the time of thermal treatment performed at T_x (646 °C) and 800 °C in: (a) $Na_{1.8}Al_{0.8}Ge_{1.2}(PO_4)_3$ and (b) $Na_2AlGe(PO_4)$ glass-ceramics. The unfilled symbols correspond to the values found for sample crystallized at 800 °C for 3 h. Lines are guide to the eyes.

The reduction in unit cell volume can be attributed to a diminution of Al content, which is also evident from the appearance of Al-containing secondary phases. Furthermore, for the sample $Na_2AlGe(PO_4)$ annealed at 800° C it was shown by ^{31}P MAS NMR spectroscopy that the effective Al content of the sample corresponds to that of composition x = 0.20 [19], stressing the extensive de-alumination. The drastic decrease in Al content of the crystalline NASICON phase together with its relatively large contribution to the inventory of crystalline material suggests that a substantial fraction of material in these samples must be glassy. This conclusion is confirmed by the appearance of an amorphous halo in the X-ray diffractogram of this sample (see Figure 1-b). This postulated vitreous phase is expected to be relatively rich in sodium, based on the deficiency of this element in the crystalline phases.

NMR Spectroscopy. ^{31}P MAS NMR spectra (see Figure 4) show partially resolved resonances centered in the spectral region between around -30 to -43 ppm, which we have recently found to be excellently described by sets of binomially distributed $P^4_{n\mathrm{Al},(4-n)\mathrm{Ge}}$ ($0 \leq n \leq 4$) species [19] reflecting the mixed ligation of phosphate species to GeO_6 and AlO_6 octahedra (see Table 2). The assignment of the P-species, appearing at progressively higher frequencies

with increasing *n*, was confirmed by $^{31}P\{^{27}Al\}$ REAPDOR experiments [19], see also Figure 6 for representative samples of the present study. Other P-containing crystalline phases are evident in the spectra: T-$AlPO_4$ (-29 ppm), $Na_7(AlP_2O_7)_4PO_4$ (-25 ppm), and various other unidentified phases giving rise to narrow signals. In addition, signal intensity is found in the spectral region between 5 and -25 ppm, which can be accounted for by several broad Gaussian components in the simulations. This spectral component signifies glassy material of considerable quantity (max 23% for x = 1.0 annealed for 3 h at T_x, compare with Table 2). Prolonging the thermal treatment or increasing the crystallization temperatures did not decrease the amount of this amorphous phase beyond 23%, but rather lead to formation of additional secondary phases and even sample decomposition. The spectrum of the x = 1.0 sample annealed for 24 h at T_x looks particularly complex, not only confirming the multiple crystalline phases identified by XRD, but also revealing a large amount of phosphate in the amorphous state, with three clearly resolvable line shape components (see Table 2). Finally, the spectra of the samples heated at 800 °C suggest substantial decomposition associated with elimination of Al from the NASICON phase in a major way. Although the chemical shifts of the dominant peaks occur near those expected for $P^4_{1Al,3Ge}$ sites, the $^{31}P\{^{27}Al\}$REAPDOR data clearly indicate that they arise from P^4_{4Ge} sites in nearly totally Al-depleted NASICON, i.e. $NaGe_2(PO_4)_3$. Also, peaks due to T-$AlPO_4$ are clearly seen in these samples (near -29 ppm), along with additional signals arising from amorphous material near -8.0 ppm. For the latter, only a weak REAPDOR effect can be noticed, suggesting that the majority of aluminium is present in one of the crystalline phases. In the sample . No signals from $Na_7(AlP_2O_7)_4PO_4$ are observed in these samples, consistent with the XRD result.

Figure 6 summarizes the ^{27}Al MAS-NMR spectra, providing clear evidence of the successively increased amount of T-$AlPO_4$ with increasing duration of the thermal treatment at T_x. Again, the sample x = 1.0 heat treated at T_x for 24 h shows unusual behavior. A very small amount (if any) of T-$AlPO_4$ is detected here; rather the spectrum gives evidence of multiple broad peaks, suggesting that Al is present in an amorphous phase. $^{27}Al\{^{31}P\}$ REDOR spectra (not shown) reveal that all of the aluminum species detected are linked to phosphorus next nearest neighbors. Furthermore, the line shape of the $Al^{(6)}$ resonance observed in the region of the NASICON phase also looks unusual, suggesting a second component not resolvable from the peak attributed to the $Al^{(6)}$ site in the NASICON phase. This component may reflect the signal of crystalline $Na_7(AlP_2O_7)_4PO_4$ that is known by X-ray diffraction to be present in this particular material, see Figure 1 and Table 1. No satisfactory simulations of the spectra could be accomplished on the basis of a distribution of quadrupolar coupling parameters (Czjzek

model) for single sites [24]. For this reason, the spectra were not simulated, but the fractions of aluminum present in the NASICON and $AlPO_4$ phases were estimated by integration analysis, leading to the results summarized in Table 3.

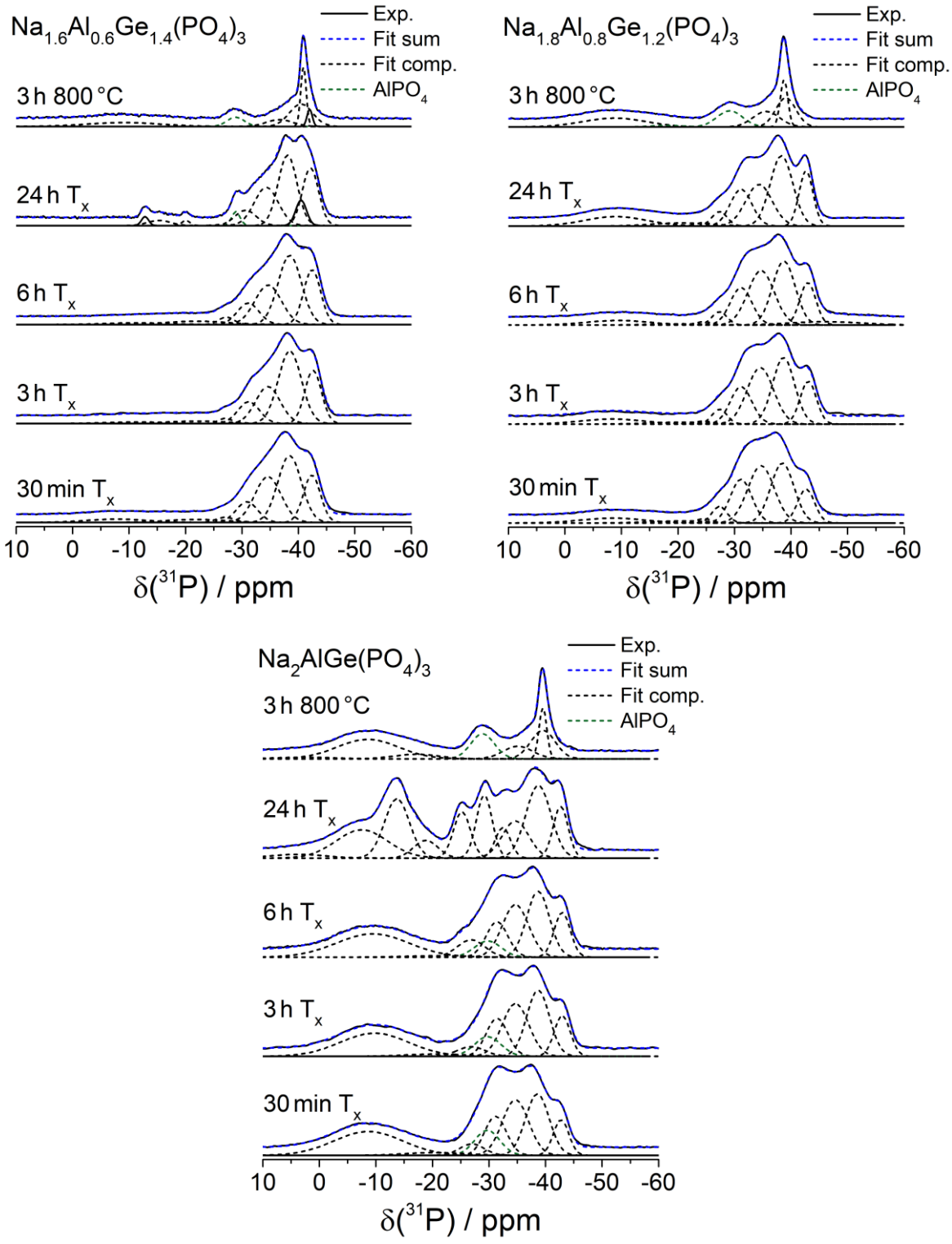

Figure 4. ^{31}P MAS NMR spectra of samples resulting from the different heat treatments performed on the parent glasses of glass-ceramics of $Na_{1.6}Al_{0.6}Ge_{1.4}(PO_4)_3$, $Na_{1.8}Al_{0.8}Ge_{1.2}(PO_4)_3$, and $Na_2AlGe(PO_4)_3$. T_x = 644 °C for x = 0.6 and 646 °C for x = 0.8 and 1.0.

Table 2. Isotropic chemical shifts δ_{CS}^{iso}, *FWHM* and area fraction of the resolved components in the ^{31}P MAS-NMR spectra of $Na_{1+x}Al_xGe_{2-x}(PO_4)_3$ glass-ceramics spectra. T_x = 644 °C for x = 0.6 and 646 °C for x = 0.8 and 1.0.

Thermal treatment	**Species**	**δ_{CS}^{iso} / ppm ± 0.5 ppm**			***FWHM* / ppm ± 0.5 ppm**			**Area fraction / % ± 2%**		
		x = 0.6	x = 0.8	x = 1.0	x = 0.6	x = 0.8	x = 1.0	x = 0.6	x = 0.8	x = 1.0
30 min @ T_X	P^4_{0Al}	-42.4	-42.7	-42.8	3.6	3.6	3.2	18	11	8
	P^4_{1Al}	-38.4	-38.5	-38.6	4.9	4.9	4.9	35	27	21
	P^4_{2Al}	-34.6	-34.7	-34.7	5.5	5.5	5.5	26	29	21
	P^4_{3Al}	-30.9	-31.2	-31.2	4.5	4.5	4.5	10	18	12
	P^4_{4Al}	-27.0	-27.3	-7.0	3.8	3.2	5.1	2	5	4
	$AlPO_4$	-	-	-29.7	-	-	5.2	-	-	9
	N7AlP*	-	-24.5	-	-	3.4	-	-	2	-
	Glass	-21.9	-20.6	-20.6	12.6	12.6	12.5	4	2	2
	Glass	-7.8	-8.5	-8.7	12.7	13.1	14.4	5	6	23
3 h @T_X	P^4_{0Al}	-42.6	-43.0	-43.0	3.5	3.4	3.4	21	14	9
	P^4_{1Al}	-38.5	-38.7	-38.7	4.9	4.6	4.7	40	28	22
	P^4_{2Al}	-34.6	-34.6	-34.7	5.1	5.5	5.5	21	29	20
	P^4_{3Al}	-31.2	-31.2	-31.4	4.5	4.5	4.5	11	16	12
	P^4_{4Al}	-27.0	-27.3	-26.8	2.8	3.2	5.7	2	4	4
	$AlPO_4$	-	-	-29.8	-	-	5.5	-	-	8
	N7AlP*	-	-24.5	-	-	3.4	-	-	1	-
	Glass	-21.9	-20.6	-20.6	12.6	12.5	12.5	3	2	2
	Glass	-11.4	-8.4	-9.7	12.8	13.0	14.3	2	6	23
6 h @ T_X	P^4_{0Al}	-42.4	-43.0	-43.0	3.6	3.3	3.4	21	13	10
	P^4_{1Al}	-38.5	-39.0	-38.7	4.9	4.7	4.7	36	28	21
	P^4_{2Al}	-34.6	-34.7	-34.7	5.5	5.5	5.5	23	27	20
	P^4_{3Al}	-31.1	-31.2	-31.4	4.5	4.5	4.5	10	15	11
	P^4_{4Al}	-27.2	-27.3	-26.8	3.2	3.2	5.7	3	4	7
	$AlPO_4$	-	-	-29.8	-	-	5.5	-	-	6
	N7AlP*	-	-24.5	-	-	3.4	-	-	1	-
	Glass	-21.9	-20.6	-20.6	12.6	12.5	12.5	5	1	1
	Glass	-11.4	-9.4	-9.4	12.8	13.1	15.1	2	6	24

	Glass	-	-46.1	-	-	15.0	-	-	5	-
24 h @ T_X	P^4_{0Al}	-42.1	-42.6	-42.7	3.4	2.9	3.1	22	14	8
	P^4_{1Al}	-38.1	-38.3	-38.7	4.0	4.7	5.2	32	30	19
	P^4_{2Al}	-34.3	-34.3	-34.7	5.0	5.5	5.5	22	21	10
	P^4_{3Al}	-30.6	-31.2	-32.5	4.4	4.5	3.2	8	15	5
	P^4_{4Al}	-26.8	-27.3	-	3.2	3.2	-	1	4	-
	$AlPO_4$	-28.9	-	-29.2	1.7	-	3.3	3	-	11
	N7AlP*	-	-24.5	-25.2	-	3.4	3.5	-	1	8
	Glass	-	-20.6	-18.8	-	12.5	5.1	-	4	5
	unknown	-	-	-13.7	-	-	5.2	-	-	16
	Glass	-	-9.0	-7.5	-	12.9	11.0	-	11	16
	Glass	-	-	4	-	-	11.1	-	-	2
	Cryst.	-40.5	-	-	2.3	-	-	6	-	-
	Cryst.	-20.1	-	-	1.7	-	-	1	-	-
	Cryst.	-15.3	-	-	4.7	-	-	3	-	-
	Cryst.	-12.8	-	-	1.5	-	-	2	-	-
3h @ 800 °C	**P^4_{0Al}**	**-40.5**	**-39.1**	**-39.6**	**4.9**	**4.2**	**5.1**	**33**	**25**	**20**
	P^4_{1Al}	**-36.6**	**-35.6**	**-35.2**	**5.5**	**5.5**	**6.2**	**12**	**17**	**10**
	P^4_{3Al}	-	-	-	-	-	-	-	-	-
	P^4_{4Al}	-	-	-	-	-	-	-	-	-
	$AlPO_4$	**-28.9**	**-29.2**	**-28.9**	**3.6**	**5.6**	**4.9**	**10**	**17**	**16**
	unknown	-	**-18.1**	**-17.2**	-	**7.2**	**9.2**	-	**2**	**6**
	Glass	**-9.0**	**-8.8**	**-8.6**	**15.4**	**13.2**	**12.8**	**18**	**24**	**34**
	Glass	-	-	**2.7**	-	-	**12.6**	-	-	**3**
	Cryst.	**-42.0**	**-38.8**	**-39.5**	**1.1**	**1.6**	**1.6**	**6**	**15**	**11**
	Cryst.	**-40.9**	-	-	**1.2**	-	-	**21**	-	-

*$Na_7(AlP_2O_7)_4PO_4$

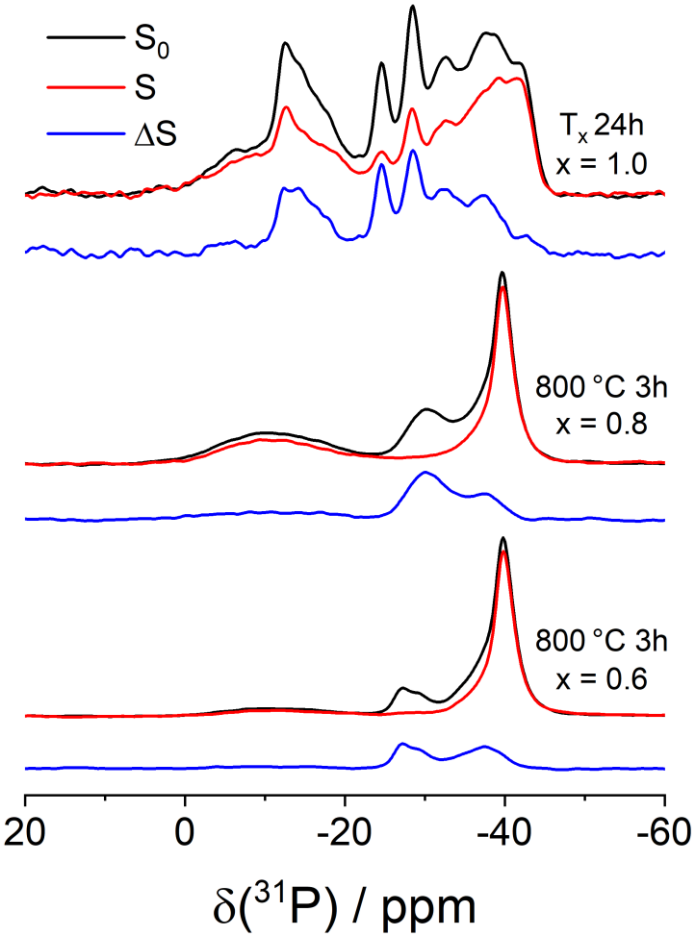

Figure 5: $^{31}P\{^{27}Al\}$ REAPDOR Fourier Transforms of representative samples. Black, red, and blue traces show the regular MAS spin echo Fourier Transforms, the spectra with dipolar recoupling for a mixing time of 2.6 ms, and the difference spectra, respectively.

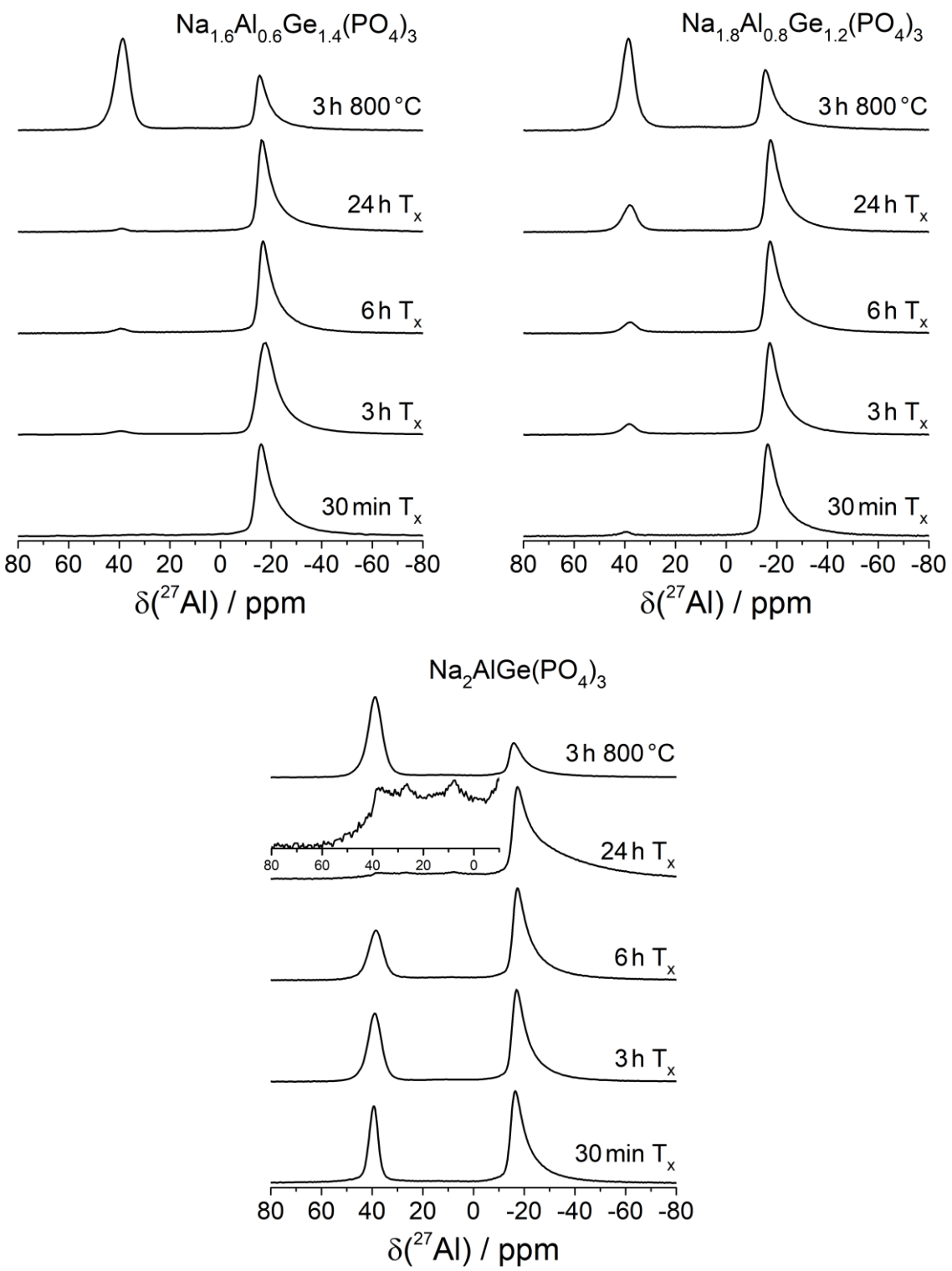

Figure 6. ^{27}Al MAS NMR spectra showing competing formation of $AlPO_4$ (≈40 ppm) against NASICON phase (≈-25 ppm) for glass-ceramics of compositions (a) $Na_{1.6}Al_{0.6}Ge_{1.4}(PO_4)_3$ (b) $Na_{1.8}Al_{0.8}Ge_{1.2}(PO_4)_3$ and (c) $Na_2AlGe(PO_4)_3$. Vertical expansion shows unresolved resonance lines, indicating $Al^{(4)}$ and $Al^{(5)}$ species from vitreous phase.

Table 3. Center of gravity δ and area fractions of the resolved components in the ^{27}Al MAS-NMR spectra of the $Na_{1+x}Al_xGe_{2-x}(PO_4)_3$ glass-ceramics.

Thermal treatment	**Species**	**δ / ppm ± 1 ppm**			**Area fraction / % ± 2%**		
		x = 0.6	x = 0.8	x = 1.0	x = 0.6	x = 0.8	x = 1.0
30 min @T_x	NASICON	-21.4	-21.4	-20.6	-	96	68
	$AlPO_4$	-	39.5	39.6	-	4	32
3 h @T_x	NASICON	-22.4	-21.0	-20.7	95	90	63
	$AlPO_4$	39.2	38.1	39.1	5	10	37
6 h @T_x	NASICON	-21.1	-22.0	-22.1	95	91	70
	$AlPO_4$	39.3	37.7	38.2	5	9	30
24 @T_x	NASICON	-26.7	-21.5	-28.6	97	80	-
	$AlPO_4$	34.8	38.0	-	3	20	-
3h @800 °C	NASICON	-18.6	-24.5	-19.6	39	48	38
	$AlPO_4$	39.2	33.6	38.7	61	52	62

Based on these results, we can conclude that prolonged heat treatment of the NASICON material results in a diminution of its Al (and Na) contents. The process we are most likely observing is the phase separation of a supersaturated solid solution formed initially by homogeneous crystallization. For example, starting with a supersaturated solution with composition x = 0.8, a diminution of the Al content by z = 0.1 is described by the process:

$$Na_{1.8}Al_{0.8}Ge_{1.2}(PO_4)_3 \rightarrow 0.24\ AlPO_4 + 0.8\ Na_{1.7}Al_{0.7}Ge_{1.3}(PO_4)_3 + \text{“}Na_{0.44}Ge_{0.16}(PO_4)_{0.36}\text{”} \quad (1)$$

The material denoted “$Na_{0.44}Ge_{0.16}(PO_4)_{0.36}$” in the above equation comprises the Na, Ge, and phosphate mass balance accompanying the formation of $AlPO_4$. We identify its ^{31}P NMR signal with the resonance near -10 ppm, which corresponds to the typical NMR signal of a sodium germanium phosphate glass [24]. Note that a reduction of Al content by z = 0.1 would lead to a 12% increase in the fractional area of the glass phase in the ^{31}P NMR spectrum and to a ^{27}Al peak area ratio (NASICON)/($AlPO_4$) of 56:24, assuming that the residual glassy phase does not contain any aluminum.

As the formation of $AlPO_4$ also entails loss of phosphate from the NASICON phase, 1 mole of NASICON containing 0.8 moles of Al results in 0.8 moles of NASICON containing

0.7 moles of Al. In general, if the Al content of 1 mole of $Na_{1.8}Al_{0.8}Ge_{1.2}(PO_4)_3$ is reduced by z, i.e, $(1-w)$ moles of NASICON phase with Al content $0.8-z$ will result, following the reaction equation

$$Na_{1.8}Al_{0.8}Ge_{1.2}(PO_4)_3 \rightarrow 3(1-w)zAlPO_4 + (1-w)Na_{1.8-z}Al_{0.8-z}Ge_{1.2+z}(PO_4)_3 + Na_{1.8-(1-w)(1.8-z)}Ge_{1.2-(1-w)(1.2+z)}(PO_4)_{3(w-z+zw)}. \quad (2)$$

This expression assumes that for any unit of $AlPO_4$ formed one unit of NASICON phase has to decompose, liberating its three equivalents of phosphate. We also assume that no re-equilibration can take place as no homogeneous melt is formed. This assumption implies that w and z are interrelated: if the amount of z is larger, the amount of $AlPO_4$, given by $3(1-w)\times z$, has to be larger as well to compensate for the Al loss. The relationship between w and z is given by the Al mass balance: $0.8 = 3(1-w)\times z + (1-w) \times (0.8-z)$, from which we can derive

$$w = 2z/(0.8 + 2z) \quad (3)$$

For example, z values of 0.05, 0.1, and 0.15 will result in w = 0.111, 0.2, and 0.27, respectively. The amount of P in the amorphous phase, f^{P}_{am}, given by $3(w-z+zw)$, will vary as well: we will get numbers of 0.20, 0.36, and 0.48, corresponding to fractional areas of 6.6 %, 12%, and 16%, respectively.

The above analysis can be done for any value of Al substitution level x. In this case the expression turns into

$$Na_{1+x}Al_xGe_{(2-x)}(PO_4)_3 \rightarrow 3(1-w)zAlPO_4 + (1-w)Na_{(1+x-z)}Al_{x-z}Ge_{(2-x+z)}(PO_4)_3 + Na_{(1+x)-(1-w)(1+x-z)}Ge_{(2-x-(1-w)(2-y+z)}(PO_4)_{3(w-z+zw)}. \quad (4)$$

while all the other calculations proceed analogously. Using eq. (3) for the general case,

$$w = 2z/(x + 2z) \quad (5)$$

we can derive the value of z from the fractional area of the ^{31}P NMR signal arising from the amorphous phase f^{P}_{am} according to:

$$z = f^{P}_{am}\times x/(2-2f^{P}_{am}) \quad (6)$$

Alternatively, we may consider getting the value of z from the integration of the ^{27}Al MAS-NMR spectra. In this case, the fractional contribution of Al contained in the form of $AlPO_4$ is given by:

$$f^{Al}_{AlPO4} = 3(1-w)z)/y = 3(1- 2z/(x+2z))/x = 3z/(x +2z), \quad (7)$$

where eq. (3) has been used. Rearrangement of this expression leads to:

$$z = f^{Al}_{AlPO4} \times x/(3-2f^{Al}_{AlPO4}) \quad (8)$$

Table 4 summarizes the z values using both the ^{31}P and the ^{27}Al NMR methods, for the samples studied as a function of thermal treatment time at T_x. Finally, the spectra obtained for samples heated at 800 °C indicate sample decomposition.

Table 4. Experimentally obtained z-values from ^{31}P MAS NMR (using equ. 6) and ^{27}Al MAS NMR (using eq. 8) for samples with x = 0.6, 0.8, and 1.0, subjected to different heat treatments. In the case of the heat treatment experiments at 800°C results from an alternative determination using eq. (9) are included in parentheses.

Thermal treatment	z from ^{31}P analysis			z from ^{27}Al analysis		
	x = 0.6	x = 0.8	x = 1.0	x = 0.6	x = 0.8	x = 1.0
30min @T_x	0.02	0.02	0.18	0.01	0.01	0.13
3h @T_x	0.02	0.02	0.15	0.01	0.03	0.16
6h @T_x	0.02	0.02	0.15	0.01	0.03	0.13
24h @T_x	0.02	0.06	0.30*	0.01	0.06	0.05*
3h @800 °C	0.07(0.15)	0.14(0.30)	0.36(0.24)	0.21	0.21	0.36

*values of z deduced from ^{31}P NMR and from ^{27}Al NMR disagree here because the decomposition mechanism discussed is not applicable for this particular sample (very little $AlPO_4$ is formed).

Inspection of Table 4 reveals that in the case of 12 out of 15 heat treated samples, the analyses from the ^{31}P and ^{27}Al MAS-NMR spectra are very well consistent with each other, thereby giving excellent support to the decomposition model. Major discrepancies between both datasets can be noted in three cases: The first two samples in which the discrepancy is seen to be major, concern the x = 0.6 and 0.8 samples heat treated for 3 h at 800 °C. In these samples, the $AlPO_4$ formed can be identified by (and quantified from) a clearly visible separate peak in the ^{31}P MAS-NMR spectrum deduced from the deconvolution of the ^{31}P MAS-NMR spectrum near -30 ppm (see Figure 4). Based on equation (4), its fractional area is given by $f^{P}_{AlPO4} = (1-w)\times z$, leading (with equ. 5) to:

$$z = f^{P}_{AlPO4}/(1-w) = x\times f^{P}_{AlPO4}/(x -2\times f^{P}_{AlPO4}) \quad (9)$$

Values for *z* deduced from equation (9) are also included in Table 5, yielding a better agreement with the data derived from ^{27}Al NMR. The third case concerns the x = 1.0 sample heat treated at T_x for 24 h. As discussed above both the XRD and the MAS-NMR data indicate that in this sample a different decomposition process prevails, involving the dominant formation of $Na_7(AlP_2O_7)_4PO_4$. Thus, the above model is not applicable here. Interestingly, as discussed in more detail below, this particular sample shows the highest electrical conductivity of all the samples.

Glass-ceramic Microstructure. Micrographs of fractured surfaces of $Na_{1+x}Al_xGe_{2-x}(PO_4)_3$ (x = 0.8 and x = 1.0) glass-ceramics crystallized at T_x (3 h, 6 h and 24 h) and 800 °C for 3 h are shown in Figure 7. The micrographs confirm the crystallization of the $Na_{1.8}Al_{0.8}Ge_{1.2}(PO_4)_3$ and $Na_2AlGe(PO_4)$ precursor glasses. In addition, one can observe a rounding of grains as the treatment time at T_x increases. However, the greatest extent of rounding is observed in samples crystallized at 800 °C for 3 h (see Figure 7 (d) and (h)).

By analyzing SEM micrographs of Figure 7 the presence of glassy phase is observed in $Na_{1.8}Al_{0.8}Ge_{1.2}(PO_4)_3$ and $Na_2AlGe(PO_4)$ samples crystallized at T_x during 6 and 24 hours and in glass-ceramics crystallized at 800° C for 3 hours. In this context, the glassy phase may improve the contact area between grains. The micrographs indicate that the contact area between grains increases as the treatment time of crystallization at T_x increases and also when the treatment temperature is raised to 800 °C, probably owing to sintering effects. Finally, the presence of vitreous phase was already evidenced also from the X-ray diffractogram of the $Na_2AlGe(PO_4)$ sample crystallized at 800 °C (see Figure 1-b).

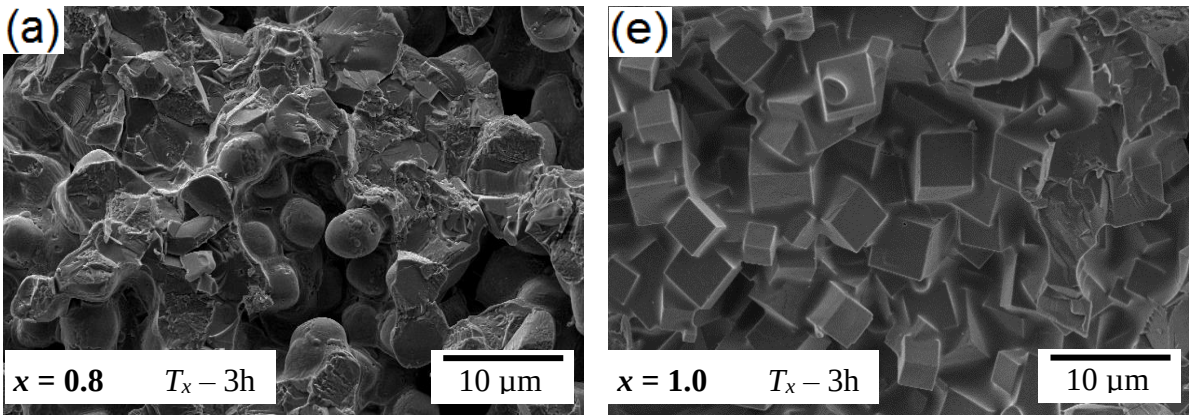

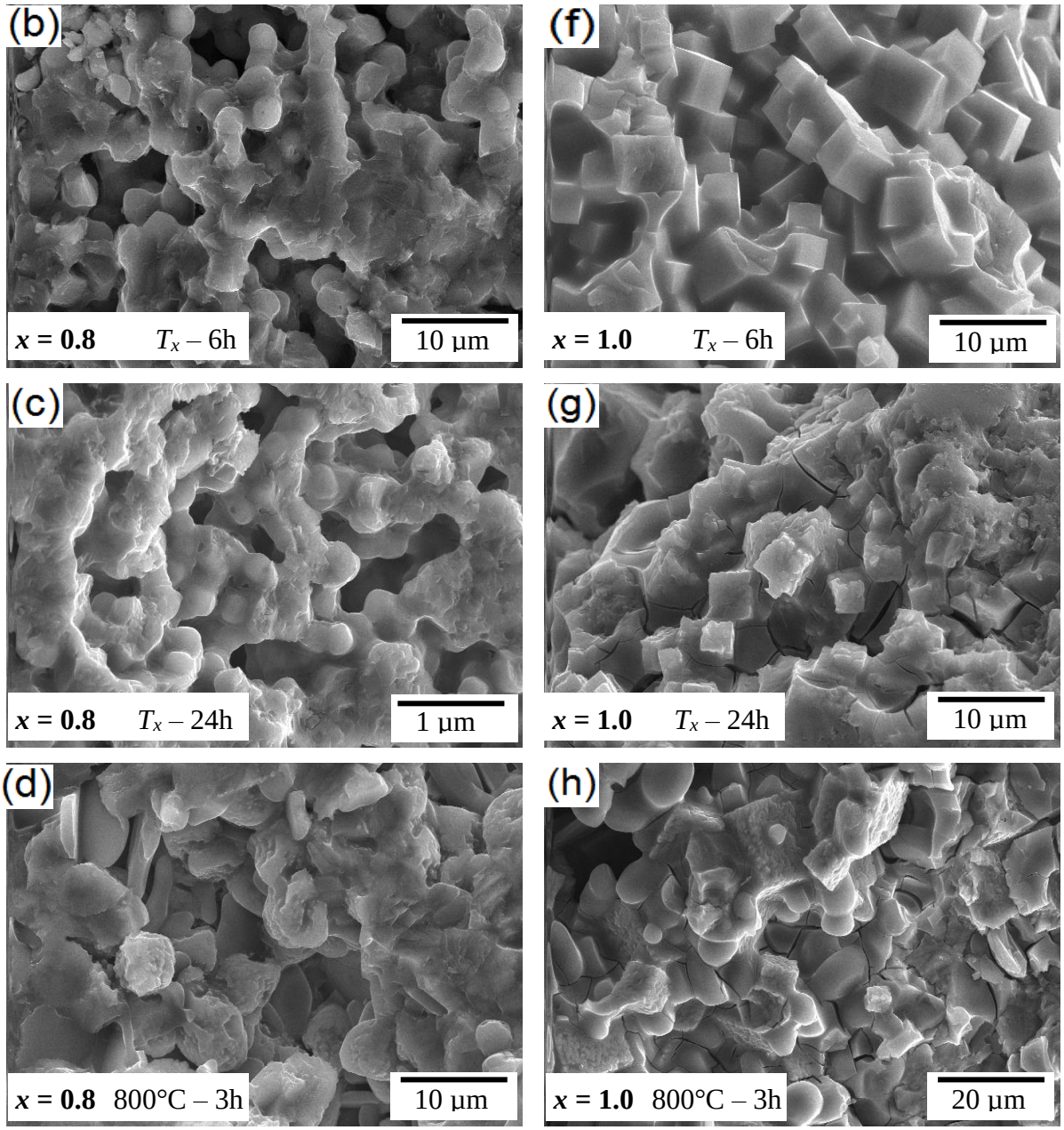

Figure 7. Microstructure of $Na_{1.8}Al_{0.8}Ge_{1.2}(PO_4)_3$ glass-ceramics crystallized at T_x = 646°C for (a) 3 h (b) 6 h (c) 24 h, and at (d) 800 °C for 3 h, and of $Na_2AlGe(PO_4)$ glass-ceramics crystallized at T_x = 646 °C for (e) 3 h (f) 6 h (g) 24 h, and at (h) 800 °C for 3 h.

Impedance Spectroscopy. Figure 8 shows an exemplary complex impedance plane plot at 100 °C for $Na_{1+x}Al_xGe_{2-x}(PO_4)_3$ (x = 0.8 and x = 1.0) glass-ceramics crystallized at T_x for 24 h. Similar results were obtained for the other samples. The straight line observed in the region of low frequencies arises from the blockage of the Na^+ ions at the sample/electrode interface and confirms that charge transport is from ionic origin. At high frequencies, only a single semicircle is observed; thus it was not possible to separate the individual responses from the grain and the grain boundary.

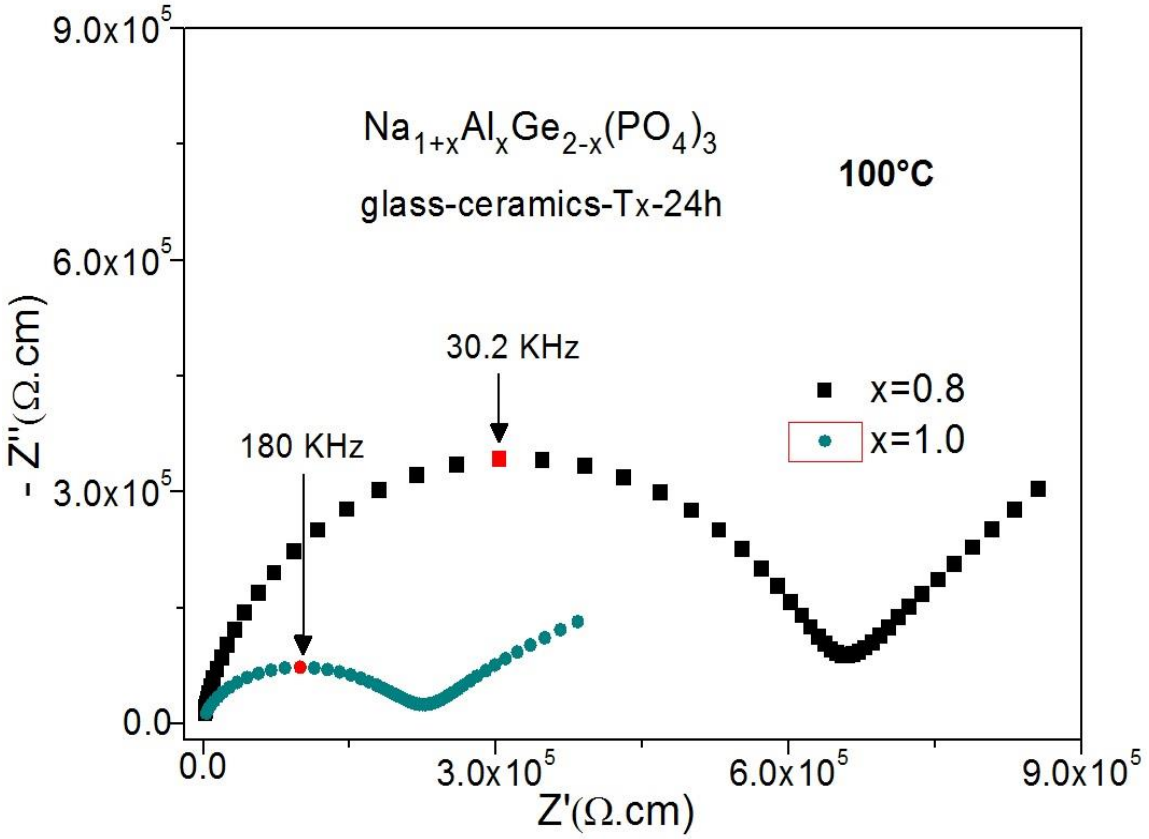

Figure 8. Complex impedance plot at 100 °C for $Na_{1+x}Al_xGe_{2-x}(PO_4)_3$ (x = 0.8 and x = 1.0) glass-ceramics obtained by annealing at T_x (646°C) for 24 h.

Ionic conductivities were calculated from the real (Z') part of the complex impedance plot taking the geometrical factor (l/S, l beeing the thickness, S the area in contact of the electrodes) into consideration. From the low frequency intercept of the semicircles with the abscissa it is possible to determine the total resistivity ρ_{Total} of the samples, from which the total ionic conductivity σ_{Total} was calculated ($\sigma_{Total} = (1/\rho_{Total})$). Figure 9 shows the Arrhenius plots obtained from temperature dependent measurements. These data were fitted to the Arrhenius equation:

$$log\ \sigma_{Total} = log\ \sigma_0 - (E_a\ /k_B T)\ \log e \qquad (10)$$

where σ_0 is the pre-exponential factor, E_a the activation energy for ionic conduction, and k_B and T are the Boltzmann constant and the absolute temperature, respectively. Table 5 summarizes the results from the corresponding linear regressions, as well as the total ionic conductivities at 300°C. Figure 10 depicts those results together with the evolution of unit cell volume as a function of heat treatment duration.

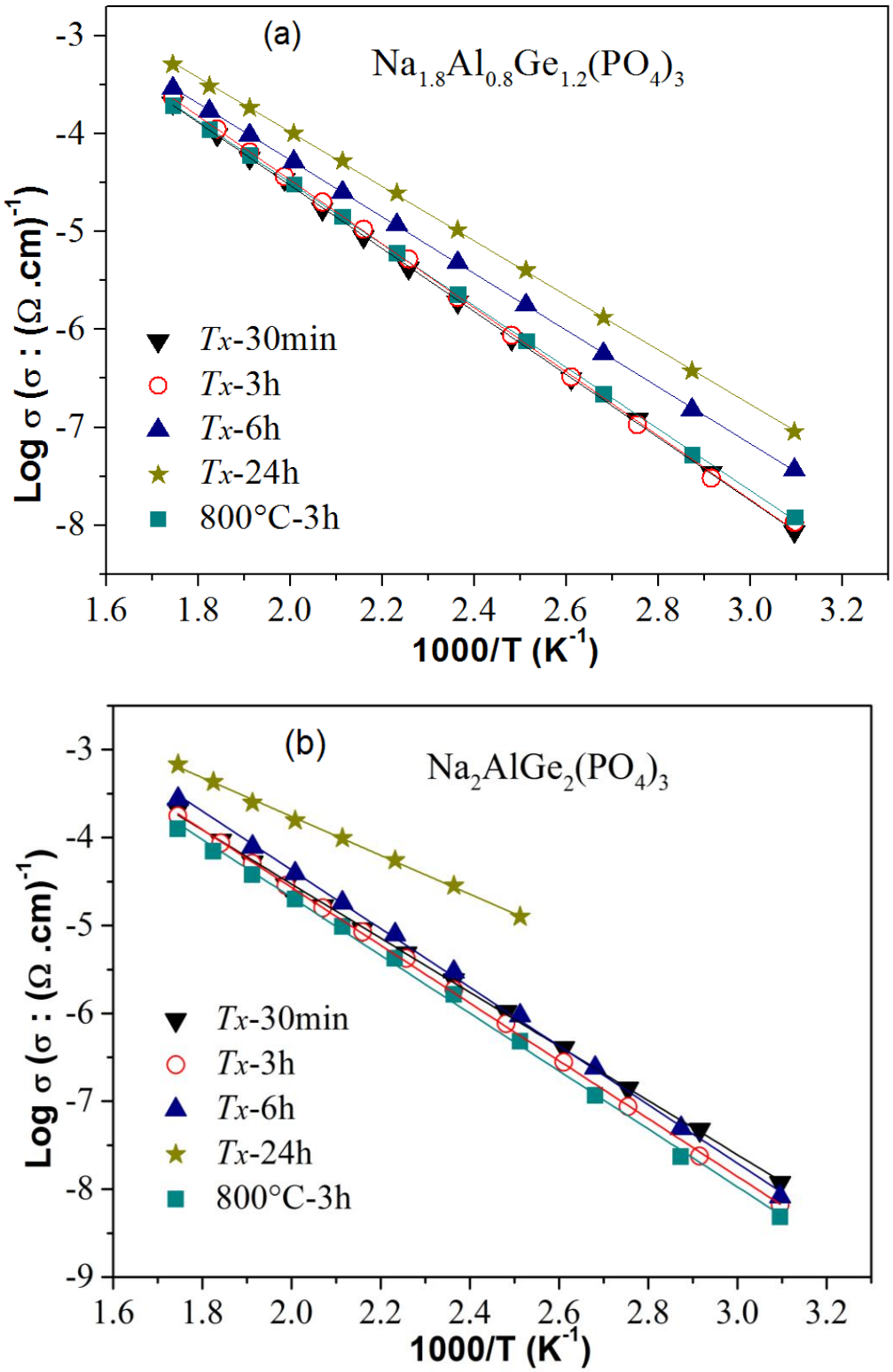

Figure 9. Temperature dependence of the ionic conductivity for $Na_{1+x}Al_xGe_{2-x}(PO_4)_3$ (x = 0.8 and x = 1.0) glass-ceramics crystallized at T_x (0.5 h, 3 h, 6 h and 24 h) and 800 °C (3 h). Lines are the linear regressions of the experimental data. Experimental uncertainties are smaller than the symbol sizes.

$$log\sigma_{Total} = log\sigma_o - (E_a / k_B T) \log e$$

Table 5. Electrical conductivities $\sigma_{300°C}$, activation energies (E_a) and $\log\sigma_0$ values for thermally treated $Na_{1+x}Al_xGe_{2-x}(PO_4)_3$ (x = 0.8 and x = 1.0). Numbers in parentheses denote the uncertainties of the linear regression of data. The conductivity values ($\sigma_{300°C}$) have an error lower than 1%.

Thermal Treatment	E_a **eV**	**log(σ_0)** (σ_0:Ω.cm)$^{-1}$	$\sigma_{300°C}$ (Ω.cm)$^{-1}$
	$Na_{1.8}Al_{0.8}Ge_{1.2}(PO_4)_3$		
T_x/30 min	0.650(4)	2.03(4)	2.0 x 10^{-4}
T_x/3 h	0.647(5)	2.06(6)	2.3 x 10^{-4}
T_x/6 h	0.574(1)	1.53(2)	3.0 x 10^{-4}
T_x/24 h	0.551(2)	1.58(3)	5.4 x 10^{-4}
800 °C/3 h	0.623(3)	1.79(3)	2.0 x 10^{-4}
	$Na_2AlGe(PO_4)_3$		
T_x/30 min	0.615(13)	1.68(4)	1.8 x 10^{-4}
T_x/3 h	0.652(4)	2.01(1)	1.9 x 10^{-4}
T_x/6 h	0.661(7)	2.31(8)	3.1 x 10^{-4}
T_x/24 h	0.437(7)	0.65(7)	6.4 x 10^{-4}
800 °C/3 h	0.653(8)	1.90(1)	1.5 x 10^{-4}

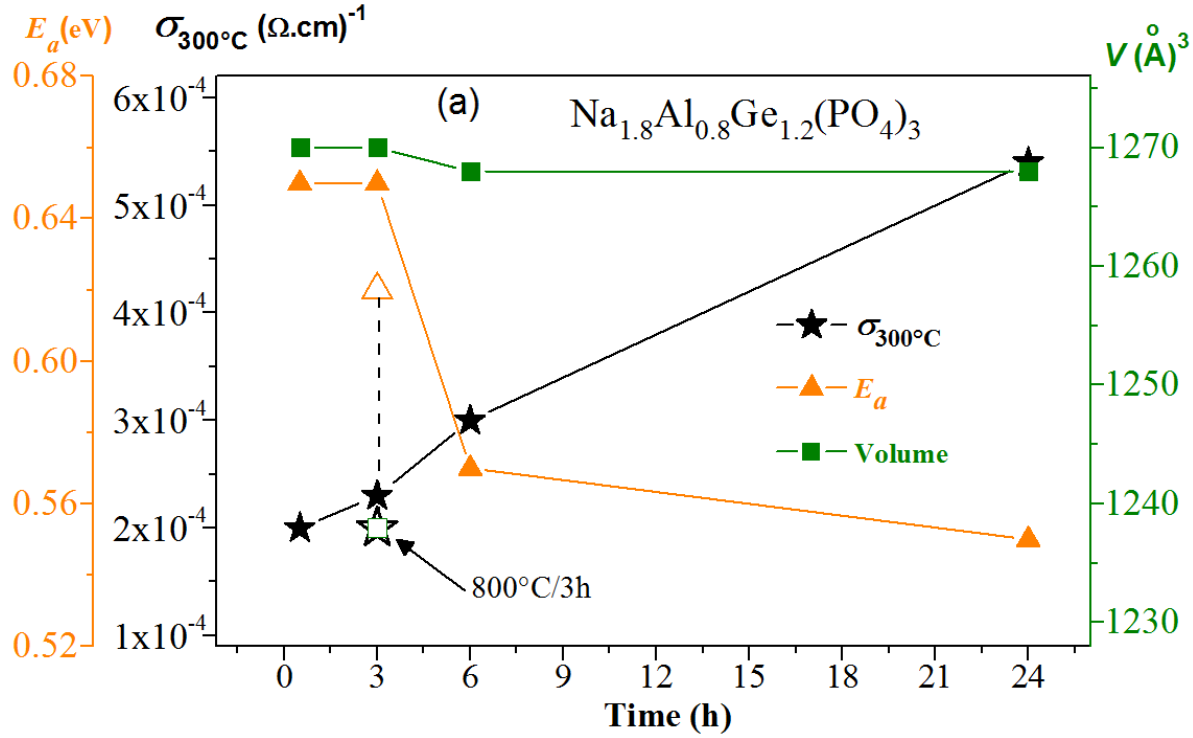

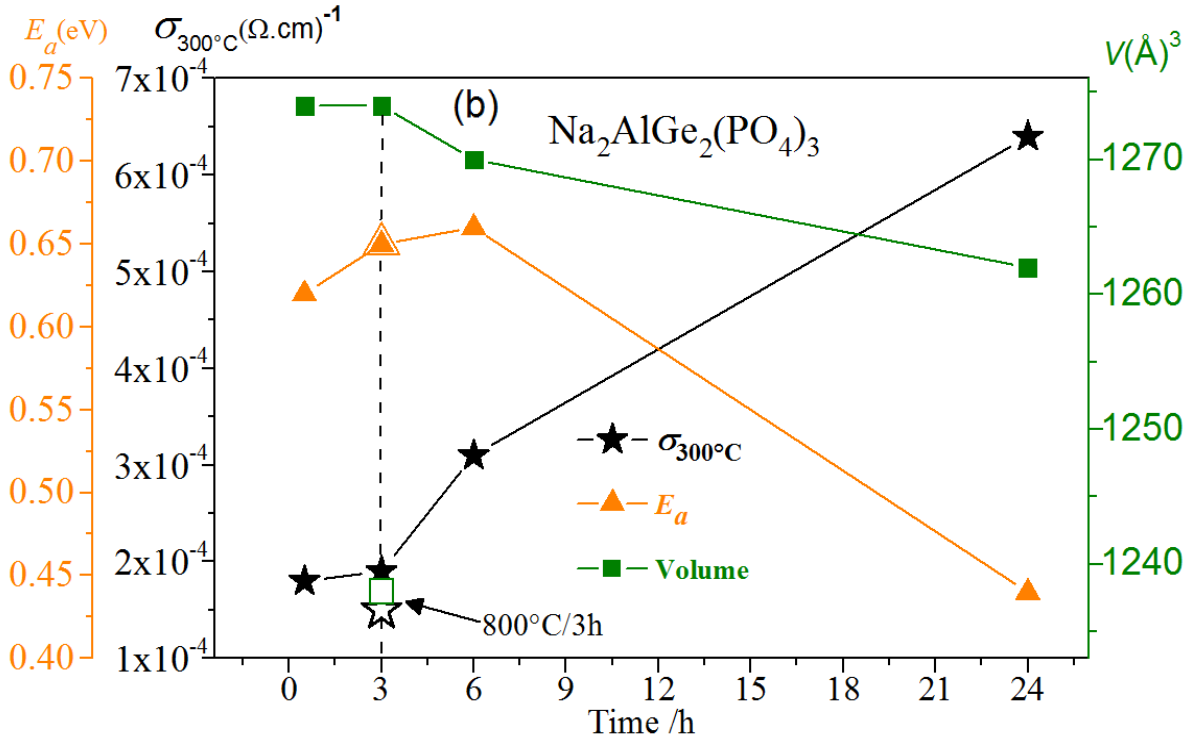

Figure 10. Ionic conductivity at 300°C ($\sigma_{300°C}$), activation energy values for ion conduction (E_a) and cell volumes of NASICON structure, as a function of the time of crystallization treatment performed at T_x (646 °C) and 800 °C for: (a) $Na_{1.8}Al_{0.8}Ge_{1.2}(PO_4)_3$ and (b) $Na_2AlGe(PO_4)$ glass-ceramics. Lines are guide to the eyes.

From the results in Figure 10 it is clearly seen that the duration of the heat treatment at 646 °C has a positive effect on ionic conductivity and activation energy, while the unit cell volume of the NASICON structure tends to decrease. This decrease is followed by a change in the unit cell composition and the emergence of new phases as discussed in previous paragraphs.

In fact, the unit cell volume of the NASICON structure of glass-ceramics $Na_{1.8}Al_{0.8}Ge_{1.2}(PO_4)_3$ crystallized at T_x for 30 minutes and for 3 hours matches the volume estimated in our previous work [19] for a sample of composition x = 0.8, obtained after a heat-treatment at T_x for 3 h. However, based on the unit cell volumes determined in [19] as a function of Al content, the glass-ceramics crystallized at T_x for 6 and 24 hours would be compositionally and structurally equivalent to an x = 0.75 sample. It is worth mentioning that there is not much variation in volume as the treatment time at T_x increases, indicating that the NASICON phase undergoes no further changes. Additionally, the ionic conductivities of $Na_{1.8}Al_{0.8}Ge_{1.2}(PO_4)_3$ samples crystallized at T_x for 0.5 h, 3 h, 6 h and 24 h, are expected to be quite similar because the compositions of the NASICON phase as inferred by NMR spectroscopy are very similar. However, Figure 10 (a), clearly shows that the conductivity increases, and the activation energy

decreases as the treatment time at T_x is increased. This finding agrees with the microstructural analysis results (previous section) which indicate that the area of contact between the grains increases as the treatment time at T_x increases, presumably due to the glassy component.

Concerning the glass-ceramics crystallized at 800 °C for 3 h, the deconvolution of the ^{31}P NMR spectra and the unit cell volume of 1238 $Å^3$ [19] suggest that this sample corresponds to a $Na_{1+x}Al_xGe_{2-x}(PO_4)_3$ glass-ceramic of composition $x = 0.2$, indicating dramatic dealumination. However, following results published by Ortiz-Mosquera [16] and Zhang [25] glass-ceramics of this composition present activation energies and ionic conductivities of about about 0.68 eV and 10^{-5} $(\Omega.cm)^{-1}$ respectively, at 300 °C. These values are slighter higher and lower than the values reported in Table 5, for samples heat treated at 800 °C/3 h. Again, the better contact between the grains (see Figure 8d) may be responsible for the unexpectedly high ionic conductivities of these samples. Alternatively, it cannot be ruled out that the residual sodium-rich glassy phase formed upon crystallization contains highly mobile ions and significantly contributes to the overall conductivity.

On the other hand, comparing the unit cell volume of $Na_2AlGe(PO_4)_3$ glass-ceramics (see Table 1) with volumes obtained by Bradtmüller et al. [19], samples crystallized at T_x for 30 minutes and 3 hours, would correspond to glass-ceramics of composition $x = 1.0$ while the samples crystallized at T_x for 6 and 24 hours would correspond to glass-ceramics with compositions $x = 0.8$ and $x = 0.6$, respectively. In this context, taking into account the trend of the ionic conductivity in $Na_{1+x}Al_xGe_{2-x}(PO_4)_3$ ($0 \leq x \leq 1.0$) glass-ceramics from results by Zhang et al [25] and by Ortiz-Mosquera et al. [16], a maximum in the curve of the ionic conductivity and a minimum in the curve of the activation energy should be observed in the $Na_2AlGe(PO_4)_3$ sample crystallized at T_x for 6 hours while a minimum in the ionic conductivity and a maximum in the activation energy should be observed for the $Na_2AlGe(PO_4)_3$ glass-ceramic crystallized at T_x for 24 hours. However, Figure 10 (b) shows that the ionic conductivity of $Na_2AlGe(PO_4)$ glass-ceramics increases as the time of treatment of crystallization at T_x increases. A fact that draws attention is the presence of the $Na_7(AlP_2O_7)_4PO_4$ phase in $Na_2AlGe(PO_4)_3$ glass-ceramics crystallized at T_x for 6 h and 24 h (see Table 1 and Figure 1). Up to now, there are no reports on the ionic conductivity of this phase and the only related work is that of Rochère at al. [26] in which materials from the $Na_7(MP_2O_7)_4PO_4$ (M= Fe, Cr) family were synthesized and electrically characterized. The authors report ionic conductivities at 300 °C in $Na_7(CrP_2O_7)_4PO_4$ and $Na_7(FeP_2O_7)_4PO_4$ materials of 5.9 x 10^{-6} $(\Omega.cm)^{-1}$ and 4.4 x 10^{-5} $(\Omega.cm)^{-1}$ respectively. Although the conductivity of the materials synthesized by Rochère is less than 10^{-4} $(\Omega.cm)^{-1}$, it

may be possible that a $Na_7(MP_2O_7)_4PO_4$ phase with M = Al, may be responsible for the increase in the ionic conductivities reported.

Based on the unit cell volume of the $Na_2AlGe(PO_4)_3$ sample crystallized at 800 °C and the values given in Table 5, we conclude that it corresponds to a glass-ceramic of composition x = 0.2. However, its activation energy is lower than those presented by Ortiz-Mosquera in [16] for an x = 0.4 sample. Also Figure 11 (b) indicates that the $Na_2AlGe(PO_4)_3$ sample crystallized at 800° C has an ionic conductivity and an activation energy comparable to that of the glass-ceramics crystallized at T_x for 3 hours. In this sense, an increased contact area may favor the ionic conductivity of this sample, despite the estimated reduced concentration of charge carriers.

The logarithm of the pre-exponential factor (log σ_0) of all the glass-ceramics studied here is in good agreement with typical values for solid electrolytes ($1 \leq \log (\sigma_0 / Scm^{-1}) \leq 3$ in most cases [15–17], consistent with a jump relaxation model for ion transport. However, an exception is observed in the $Na_2AlGe(PO_4)_3$ sample crystallized at T_x for 24 h which is the most conductive glass-ceramic of the present study. The pre-exponential factor depends on many factors such as the homogeneity of the sample. Since this sample has many secondary phases (see Figure 1 (b)), it can be suggested that the multi-phase character of this sample may be responsible for the low pre-exponential factor in this case.

It is noteworthy, that among all the glass-ceramics investigated here, the most conductive ones are those crystallized at T_x= 646 °C for 24 hours. These samples also exhibit the lowest activation energies (0.551 eV for $Na_{1.8}Al_{0.8}Ge_{1.2}(PO_4)_3$ and 0.437 eV for $Na_2AlGe(PO_4)$). In the case of $Na_2AlGe(PO_4)_3$, samples heat treated under these conditions have ionic conductivities exceeding the highest values reported by Zhang et al. (3.8×10^{-4} $(\Omega.cm)^{-1}$) and by Ortiz-Mosquera (4.3×10^{-4} $(\Omega.cm)^{-1}$). We conclude that the thermal treatments performed at 646 °C for 24 hours were the most effective measure in the optimization of ionic conductivity, despite the fact that this treatment does not lead to a maximized fraction of NASICON phase. Thus, the results of the present study indicate that other factors (interparticle contacts, presence of secondary ion-conducting phases) play an important role in controlling the ionic conductivity of sodium-conducting NASICON glass ceramics.

Conclusions

In conclusion, the results of the present study indicate that the composition of the NASICON phase in $Na_{1+x}Al_xGe_{2-x}(PO_4)_3$ glass-ceramics changes with the duration of isothermal heat-treatments at temperatures $T \geq T_x$. While larger amounts of Na^+ and Al^{3+} can

be incorporated within an initially homogeneous NASICON phase, extended annealing at T_x results in progressive segregation of $AlPO_4$, accompanied by the formation of some amorphous material. Thus, crystallization initially produces a super-saturated NASICON solid solution, whose composition and structure evolves with time to a more stable composition, with lower Al-content. We have developed a quantitative description of this process, based on solid state NMR results. Annealing the sample at 800 °C results in extensive de-alumination of the NASICON phase. Notwithstanding this decomposition, our study indicates that the ionic conductivity and activation energy of ion conduction are affected to a much lesser extent than expected on the basis of the Al content (x) of the remaining NASICON phase. The highest ionic conductivity is observed in a sample of $Na_2GeAl(PO_4)_3$ annealed at T_x for 24 hours. XRD and solid-state NMR indicate that this material features a significant amount of crystalline $Na_7(AlP_2O_7)_4PO_4$ and Na-containing amorphous phase as well, whereas crystalline T-$AlPO_4$ is not detectable. These results indicate that the secondary crystalline and glassy phases formed alongside this equilibration process make important contributions to ion transport in these glass ceramics. The contributions could be direct, via ionic motion in the (relatively sodium-rich) secondary phases or indirect, with the amorphous phases facilitating inter-particle contacts promoting ion transport.

Acknowledgments

This work was supported by the Center of Research, Technology and Education in Vitreous Materials (CeRTEV), via FAPESP, (process number 2013/07793-6) via the CEPID program, the Coordenação de Aperfeiçoamento de Pessoal de Nível Superior - (CAPES), Brazil, Finance Code 001. H.B. also acknowledges support from the Deutsche Forschungsgemeinschaft.

References

[1] M.D. Slater, D. Kim, E. Lee, C.S. Johnson, Sodium-ion batteries, Adv. Funct. Mater. 23 (2013) 947–958. doi:10.1002/adfm.201200691.

[2] K.B. Hueso, M. Armand, T. Rojo, High temperature sodium batteries: Status, challenges and future trends, Energy Environ. Sci. 6 (2013) 734–749. doi:10.1039/c3ee24086j.

[3] D. Kundu, E. Talaie, V. Duffort, L.F. Nazar, The Emerging Chemistry of Sodium Ion Batteries for Electrochemical Energy Storage Angewandte, (2015) 3431–3448. doi:10.1002/anie.201410376.

[4] Y. Noguchi, E. Kobayashi, L.S. Plashnitsa, S. Okada, J. Yamaki, Electrochimica Acta

Fabrication and performances of all solid-state symmetric sodium battery based on NASICON-related compounds, Electrochim. Acta. 101 (2013) 59–65. doi:10.1016/j.electacta.2012.11.038.

[5] F. Lalère, J.B. Leriche, M. Courty, S. Boulineau, V. Viallet, C. Masquelier, V. Seznec, An all-solid state NASICON sodium battery operating at 200°C, J. Power Sources. 247 (2014) 975–980. doi:10.1016/j.jpowsour.2013.09.051.

[6] G. Li, Z. Yang, Y. Jiang, C. Jin, W. Huang, X. Ding, Nano Energy Towards polyvalent ion batteries : A zinc-ion battery based on NASICON, Nano Energy. 25 (2016) 211–217. doi:10.1016/j.nanoen.2016.04.051.

[7] N. Anantharamulu, K.K. Rao, G. Rambabu, B.V. Kumar, V. Radha, M. Vithal, A wide-ranging review on Nasicon type materials, (2011) 2821–2837. doi:10.1007/s10853-011-5302-5.

[8] M. Guin, F. Tietz, Survey of the transport properties of sodium superionic conductor materials for use in sodium batteries, J. Power Sources. 273 (2015) 1056–1064. doi:10.1016/j.jpowsour.2014.09.137.

[9] D. Zhao, Z. Xie, J.M. Hu, H. Zhang, W. long Zhang, S.L. Yang, W.D. Cheng, Structure determination, electronic and optical properties of NaGe2P3O12 and Cs2GeP4O13, J. Mol. Struct. 922 (2009) 127–134. doi:10.1016/j.molstruc.2009.01.009.

[10] H. Eckert, A. Candida, M. Rodrigues, Ion-conducting glass-ceramics for energy-storage applications, (2019) 206–212. doi:10.1557/mrs.2017.30.

[11] F.J. Berry, N. Costantini, L.E. Smart, Synthesis and characterisation of Cr3+-containing NASICON-related phases, Solid State Ionics. 177 (2006) 2889–2896. doi:10.1016/j.ssi.2006.08.019.

[12] F.E. Mouahid, M. Bettach, M. Zahir, P. Maldonado-Manso, E.R. Bruque, S.Losilla, M.A.G. Aranda, Crystal chemistry and ion conductivity of the Na1 + xTi2 − xAlx(PO4)3 ($0 \leq x \leq 0.9$) NASICON series, J. Mater. Chem. 10 (2000) 2748–2753. doi:10.1039/b004837m.

[13] P. Maldonado-Manso, M.A.G. Aranda, S. Bruque, J. Sanz, E.R. Losilla, Nominal vs. actual stoichiometries in Al-doped NASICONs: A study of the Na1.4Al0.4M1.6(PO4)3 (M = Ge, Sn, Ti, Hf, Zr) family, Solid State Ionics. 176 (2005) 1613–1625. doi:10.1016/j.ssi.2005.04.009.

[14] J. Fu, Fast Li+ ion conducting glass-ceramics in the system Li2O–Al2O3–GeO2–P2O5, Solid State Ionics. 104 (1997) 191–194. doi:10.1016/s0167-2738(97)00434-7.

[15] J.L. Narváez-Semanate, A.C.M. Rodrigues, Microstructure and ionic conductivity of Li1

+ xAl xTi2-x(PO4)3 NASICON glass-ceramics, Solid State Ionics. 181 (2010) 1197–1204. doi:10.1016/j.ssi.2010.05.010.

[16] J.F. Ortiz-Mosquera, A.M. Nieto-Muñoz, A.C.M. Rodrigues, Precursor glass stability, microstructure and ionic conductivity of glass-ceramics from the Na1+xAlxGe2–x(PO4)3 NASICON series, J. Non. Cryst. Solids. 513 (2019) 36–43. doi:10.1016/j.jnoncrysol.2019.03.008.

[17] A.M. Cruz, E.B. Ferreira, A.C.M. Rodrigues, Controlled crystallization and ionic conductivity of a nanostructured LiAlGePO4 glass–ceramic, J. Non. Cryst. Solids. 355 (2009) 2295–2301. doi:10.1016/j.jnoncrysol.2009.07.012.

[18] D. Safanama, R.P. Rao, H.E.A. Brand, N. Sharma, S. Adams, Structural evolution of NASICON-type Li 1+x Al x Ge 2−x (PO 4) 3 using in situ synchrotron X-ray powder diffraction, J. Mater. Chem. A. 4 (2016) 7718–7726. doi:10.1039/c6ta00402d.

[19] H. Bradtmüller, A.M. Nieto-Muñoz, J. Ortiz-Mosquera, A.C.M. Rodrigues, H. F.Eckert, Glass-to-crystal transition in the NASICON glass-ceramic system Na1+xAlxM2−x(PO4)3 (M=Ge, Ti), J. Non. Cryst. Solids. 489 (2017) 91–101. doi:10.1016/j.jnoncrysol.2017.10.057.

[20] Oxford Cryosystems, Crystallographica Search-Match, J. Appl. Crystallogr. 32 (1999) 379–380. doi:10.1107/s0021889899004124.

[21] A.A. Coelho, J. Evans, I. Evans, A. Kern, S. Parsons, The TOPAS symbolic computation system, Powder Diffr. 26 (2011) S22–S25. doi:10.1154/1.3661087.

[22] A. Belkly, M. Helderman, V.L. Karen, P. Ulkch, New developments in the Inorganic Crystal Structure Database (ICSD): Accessibility in support of materials research and design, Acta Crystallogr. Sect. B Struct. Sci. 58 (2002) 364–369. doi:10.1107/S0108768102006948.

[23] D. Massiot, F. Fayon, M. Capron, I. King, S. Le Calvé, B. Alonso, J.O. Durand, B. Bujoli, Z. Gan, G. Hoatson, Modelling one- and two-dimensional solid-state NMR spectra, Magn. Reson. Chem. 40 (2002) 70–76. doi:10.1002/mrc.984.

[24] J.B. d'Espinose de Lacaillerie, C. Fretigny, D. Massiot, MAS NMR spectra of quadrupolar nuclei in disordered solids: The Czjzek model, J. Magn. Reson. 192 (2008) 244–251. doi:10.1016/j.jmr.2008.03.001.

[25] Q. Zhang, Z. Wen, Y. Liu, S. Song, X. Wu, Na+ ion conductors of glass–ceramics in the system Na1+xAlxGe2−xP3O12(0.3≤x≤1.0), J. Alloys Compd. 479 (2009) 494–499. doi:10.1016/j.jallcom.2008.12.106.

[26] M. de la Rochère, K. A., F. D'Yvoire, E. Bretey, (Received November 5 , 1984 ;

Communicated by P . Hagenmuller), Powder Diffr. 20 (1985) 27–34.